BIOCHEMISTRY

Single-cell chemoproteomics identifies metastatic activity signatures in breast cancer

Kavya Smitha Pillai[1,2]†, Olivia Laxton[1,2,3]†, Gang Li[1,2], Jing Lin[2,3], Olga Karginova[4], Rita Nanda[4], Olufunmilayo I. Olopade[4], Savaş Tay[2,3]*, Raymond E. Moellering[1,2]*

Protein activity state, rather than protein or mRNA abundance, is a biologically regulated and relevant input to many processes in signaling, differentiation, development, and diseases such as cancer. While there are numerous methods to detect and quantify mRNA and protein abundance in biological samples, there are no general approaches to detect and quantify endogenous protein activity with single-cell resolution. Here, we report the development of a chemoproteomic platform, single-cell activity-dependent proximity ligation, which uses automated, microfluidics-based single-cell capture and nanoliter volume manipulations to convert the interactions of family-wide chemical activity probes with native protein targets into multiplexed, amplifiable oligonucleotide barcodes. We demonstrate accurate, reproducible, and multiplexed quantitation of a six-enzyme (Ag-6) panel with known ties to cancer cell aggressiveness directly in single cells. We further identified increased Ag-6 enzyme activity across breast cancer cell lines of increasing metastatic potential, as well as in primary patient-derived tumor cells and organoids from patients with breast cancer.

INTRODUCTION

Recent advances in multi-omics profiling methods and platforms have enabled the detection and quantitation of biomolecules involved in signal regulation at each step of the central dogma. DNA- and RNA-centered measurements have led the way due to the maturity and availability of enzymatic oligonucleotide amplification, reverse transcription, and sequencing technologies (*1*–*4*). One area of particular growth has been the development of single-cell transcriptional profiling technologies and their application in diseases like cancer (*5*), where heterogeneity exists within the tumor compartment, circulating tumor cell populations, and the surrounding cells of the tumor microenvironment. While these technologies are powerful, it is well characterized that there are poor correlations between DNA, RNA, and protein levels in model organisms (*6*, *7*), including humans (*8*, *9*), and even within the same clinical samples (*10*). Therefore, the development of high-resolution technologies capable of interrogating protein abundance, and if possible, protein activity state, remains an area of great importance.

The functional states of endogenous proteins are subject to extensive posttranslational regulation, which can result in significant disparity between protein abundance and protein activity. These regulatory events include posttranslational modifications (*11*, *12*), protein-protein (*13*, *14*) or protein-metabolite interactions (*15*, *16*), impacts of the surrounding chemical environment (*17*, *18*), spatial compartmentalization (*19*), and even mechanical forces (*20*). As a result, activity-based protein profiling methods have been developed to integrate chemical probes upstream of liquid chromatography tandem mass spectrometry (LC-MS/MS) or gel-based protein separation to specifically detect and quantify only active subpopulations of the proteome of interest (*21*–*23*). Family-wide chemical proteomic probes are particularly powerful as they can report on the activity of large swaths of the active proteome simultaneously, with published examples available for numerous enzyme families, general reactive functionalities and specific posttranslational modifications (*22*, *24*–*32*). While ideal for discovery-mode profiling, the use of gel- and MS-based detection strategies requires relatively large cellular sample input, extensive and expensive processing workflows, relatively low sample throughput, and may lack the sensitivity to detect many low-abundance proteins or proteoform pools. Moreover, many of the contextual features of cellular samples, such as heterogeneity and spatial relationships, are completely lost in the homogenization of thousands to millions of cells during sample processing. Together, these limitations can prevent the application of activity-based profiling methods to areas of fundamental and translational science.

To address some of these limitations, we recently developed an alternative chemical proteomic detection platform, activity-dependent proximity ligation (ADPL), which integrates modular, family-wide chemical probes (including those previously reported for MS- and gel-based readouts) (*23*) with proximity-dependent oligonucleotide amplification (*33*) to quantify active proteins in native contexts with high spatial resolution (*34*, *35*). Specific probe-protein complexes can be detected by protein recognition reagents (e.g., antibody-oligonucleotide) and probe-directed (e.g., streptavidin-oligonucleotide) recognition elements to convert the probe-target labeling event into barcoded oligonucleotide amplicons. One can "write" and "read" barcoded amplicons directly on fixed cells or tissues for quantitative visualization of active proteins with fluorescence imaging techniques. Alternatively, barcoded amplicons can be templated and quantified in whole cell proteome (e.g., lysate) via soluble (s)ADPL for ultrasensitive quantification by reverse transcription quantitative polymerase chain reaction (RT-qPCR; fig. S1). This latter approach permits multiplexed measurement of many active protein targets with streamlined sample processing, minimal sample input, and high quantitative accuracy. In principle, the signal amplification and barcoding afforded by sADPL could be extended to detect distinct active proteins, or multiplexed activity "signatures" from isolated single cells, regardless of their origin. However, in its current form, sADPL is

[1]Department of Chemistry, The University of Chicago, Chicago, IL 60637, USA. [2]Institute for Genomics and Systems Biology, The University of Chicago, Chicago, IL 60637, USA. [3]Pritzker School of Molecular Engineering, The University of Chicago, Chicago, IL 60637, USA. [4]Center for Clinical Cancer Genetics and Global Health, Department of Medicine, The University of Chicago, Chicago, IL 60637, USA.
*Corresponding author. Email: tays@uchicago.edu (S.T.); rmoellering@uchicago.edu (R.E.M.)
†These authors contributed equally to this work.

limited by manual sample processing and concomitant issues with practical volume manipulations and sensitivity.

Herein, we present an automated microfluidic pipeline for single-cell isolation and "on-chip" sADPL processing for multiplexed protein activity measurements on isolated single cells. By applying the single-cell ADPL (scADPL) workflow to cancer cell lines and samples from patients with primary breast cancer (BC), we identify a cancer-aggressiveness activity signature that correlates with metastatic BC progression.

RESULTS

Quantifying active proteins in isolated single cells with scADPL

Soluble ADPL is capable of quantifying active protein subpopulations in as little as 10 pg of whole proteome (*36*). Published estimates of the total protein content within a single epithelial human cell (e.g., a HeLa cell) is approximately 2 ng (*37*). We therefore reasoned that it should be possible to perform sADPL measurements, perhaps for many targets in parallel, at the single-cell level. We first sought to automate, streamline, and optimize our sADPL method by developing a microfluidic device–based protocol capable of (i) isolating, culturing, and imaging live single cells from diverse biological samples; (ii) automated delivery and manipulation of nanoliter volumes to achieve suitable working proteome concentrations (*36*) for optimal ADPL barcoding and amplification; and (iii) reduce dead volume to maximize sensitivity and reproducibility (Fig. 1A) (*38*). We therefore adapted a previously developed microfluidic device (*38*) for single-cell isolation and chemical processing of cells, and then developed and integrated chemical protocols that enabled single-cell protein activity measurements in each cell. In our on-chip scADPL workflow, single cells, pulse labeled with ADPL-compatible activity probes, are subjected to capture in individual nanochambers, where they are lysed and incubated with ADPL barcoding reagents (Fig. 1A and fig. S1). This system requires compatibility of all reagents for "one-pot" proximity barcoding and amplification within the whole proteome, as we validated previously for sADPL, followed by amplicon retrieval and quantification by qPCR or digital droplet PCR (ddPCR; Fig. 1A).

Building on our previous microfluidic designs (*38*), we first tested the scADPL workflow for detection of both a soluble protease (CTSL) using an ADPL-compatible cathepsin family-wide chemical probe (Cat-Bio) (*36*, *39*) and an integral membrane hydrolase (NCEH1) with an ADPL-compatible serine hydrolase family-wide chemical probe (FP-Bio) (*22*, *23*, *33*, *36*) in single SKOV3 cancer cells. We first performed

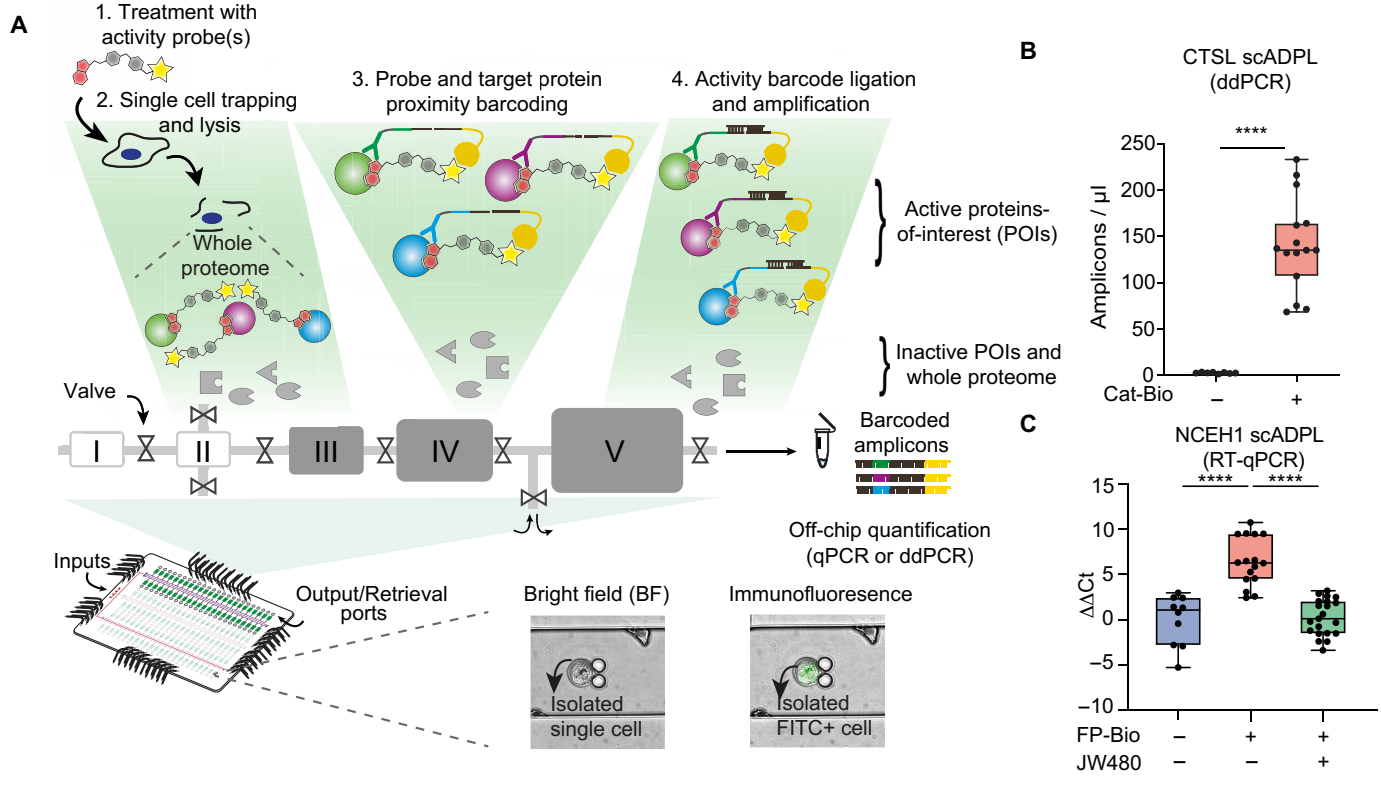

Fig. 1. Microfluidics-coupled single-cell activity-dependent proximity ligation (scADPL). (**A**) Microfluidic chip design for automated scADPL. One unit of assay chambers is shown in detail (not to scale), including input fluid artery (I); single-cell trapping chamber (II); cell lysis chamber (III); proximity barcoding element incubation in whole proteome (IV); and proximity barcode ligation (V). Output retrieval containing ligated amplicons can be quantified by off-chip qPCR. Bright-field and fluorescence micrograph image shows isolation of a single cell labeled with FITC-labeled anti-CD45 antibody in an assay chamber (arrow tail). (**B**) ddPCR quantification of relative cathepsin L (CTSL) activity in isolated SKOV3 cells treated with 5 µM cathepsin targeting probe (Cat-Bio) or vehicle only–treated cells. (**C**) qPCR quantification of relative NCEH1 activity in isolated SKOV3 cells treated with 2 µM serine hydrolase family targeting probe (FP-Bio), with or without 2 µM selective NCEH1 small-molecule inhibitor (JW480) or vehicle only–treated cells. Box plots represent the median and quartiles; the whiskers go down to the smallest values and the highest values. Individual data points each represent a single measurement from an isolated cell. Data are representative of $n = 2$ (B) and $n = 3$ (C) independent biological replicates. Student's two-way *t* test, ****$P < 0.0001$.

validation of optimal conditions for scADPL, including streptavidin-oligo and antibody-oligo concentrations, lysis buffers, chip temperature, and ADPL barcoding conditions, arriving at a working window that was similar to that found in our previous "bulk" sADPL assay (*36*), albeit scaled down for volume (fig. S2). Family-wide probe concentrations and durations mirrored previous imaging and soluble ADPL studies (*36*, *39*). Using these conditions, we used scADPL to measure CTSL signal in isolated SKOV3 cells using ddPCR to detect and quantify barcoded amplicons. The average scADPL signal was 54-fold higher in Cat-Bio–treated cells relative to vehicle-treated cells, confirming that single-cell activity measurements could be detected by ddPCR (Fig. 1B). In parallel, we measured the scADPL signal for active NCEH1 in cells treated with FP-Bio or vehicle followed by qPCR quantification, resulting in a similar ~64-fold higher signal. Moreover, pretreatment of FP-Bio–treated cells with a selective NCEH1 inhibitor, JW480, significantly inhibited the signal increase, confirming the target specificity of the scADPL signal similar to our previously reported imaging and bulk sADPL systems (Fig. 1C) (*33*, *36*). As chemical probes like FP-bio are intentionally developed to interrogate families of tens to hundreds of protein targets, it is important to validate target-selective signal generation through inhibitors such as JW480. ddPCR measurement of NCEH1-dependent scADPL signal clearly showed probe-dependent signal production but with significantly lower signal-to-noise ratio relative to qPCR (fig. S2). Because we intended to use a detection and quantification method that is robust across different types of protein targets and amenable to multiplexing, we chose to use qPCR from that point forward. Collectively, these data identified general working windows for automated, single-cell ADPL and supported the potential for robust measurement of active proteins in whole, soluble proteome from isolated single cells with scADPL.

Multiplexed activity profiling in isolated single cells

After establishing the ability to measure active proteins quantitatively and sensitively in single cells with scADPL, we sought to test whether our scADPL pipeline was capable of multiplexed quantification of active target proteins. We focused on profiling a six-enzyme panel composed of four serine hydrolase family members (NCEH1, MGLL, FAAH, and uPA) and two cathepsins (CTSL and CTSB) with strong ties to cancer cell aggressiveness (Ag6 panel) (*36*, *40*–*44*). Because of the family-wide targeting of Cat-Bio and FP-Bio, this panel can be profiled by pulsed labeling of single cells with just these two probes. We adapted our single-plex scADPL workflow to include orthogonal, target-specific barcoding sequences within the forward primer sequence to enable universal ligation and amplification of all target enzymes, but target-specific quantification on unique barcode channels in qPCR; all other conditions from our single-plex workflow remained the same (fig. S2). We first performed probe versus no-probe experiments in SKOV3 cells and measured the activity signal of each target in the Ag6 panel from the same cell (i.e., six orthogonal qPCR measurements of different targets from every isolated cell). Highly significant and target-dependent activity levels were measured, with relatively high activity for NCEH1, MGLL, and CTSL (>20-fold over no probe background) and lower but detectable activity for FAAH, CTSB, and uPA (Fig. 2A). The specificity of these multiplexed scADPL measurements was confirmed using selective inhibition of NCEH1 by JW480, which inhibited NCEH1-specific scADPL signal by >90% but had no significant effect on the scADPL activity measurement of the other targets (Fig. 2B). Multiplexed scADPL quantification was reproducible across replicate samples run on different microfluidic devices and subsequent days (Fig. 2C; Pearson $r = 0.9981$). In addition, quantification was accurate relative to known activity of the Ag-6 panel in SKOV3 measured by bulk sADPL (i.e., aggregate of many cells) (*36*) and previously published imaging ADPL studies (*33*). We also compared the activity signatures from our bulk sADPL pipeline to that from our scADPL pipeline and observed a highly significant correlation between the data collected via these two workflows. (Fig. 2D; Pearson $r = 0.9288$). Together, these experiments validate the potential for multiplexed profiling of protein activity states within single cells, which enables the identification of single target or aggregate activity signatures for molecular phenotyping of diverse cellular samples.

Multiplexed scADPL detects heterogeneous activity signatures within and between different cell lines

Averaged activity signatures obtained via traditional (e.g., gel or mass spectrometry based) as well as our bulk sADPL method require mixtures of thousands (via the sensitivity afforded by sADPL) to millions of cells upstream of the activity-based processing and analysis workflow. This fundamentally limits the ability to profile many sample types, such as small patient samples or circulating cells, and precludes bona fide measurement of protein activity within single cells. While useful for intersample comparisons, the inherent heterogeneity within clinical samples cannot be detected or quantified using these workflows. We therefore sought to test whether our scADPL workflow can be used to reliably detect specific protein activity differences and aggregate signatures between distinct single-cell populations. We compared disparate signatures both between and within cell lines. To do so, we compared single-cell activity profiles of the 6-enzyme panel in cells originating from different tissues [kidney human embryonic kidney (HEK) 293T versus ovarian SKOV3 cells], as well as tissue-matched cell lines with established differences in aggressive phenotypes (ovarian cancer SKOV3 versus OVCAR3). We observed significant differences in the aggressive enzyme activity of all targets in SKOV3 relative to HEK293T cells (Fig. 3A). Multiplexed scADPL analysis also identified significantly increased activity of all Ag6 enzymes, with the highest change in NCEH1, in SKOV3 cells relative to the less aggressive OVCAR3 population (Fig. 3B). The scADPL-generated activity profiles of the ovarian cancer cell lines were in agreement with previous measurements made by imaging or soluble bulk ADPL, as well as gel profiling (*36*). We compared these relative active protein measurements to standardized mRNA abundance (via the Human Protein Atlas Database). While several targets exhibited similar trends between mRNA and active protein levels, others, like FAAH and CTSB, demonstrated discordant profiles that could stem from posttranscriptional and posttranslational regulation of activity (Fig. 3C and fig. S3). Last, a unique feature of the single-cell activity profiles acquired with scADPL is the ability to quantify protein activity heterogeneity between single cells of the same origin. This is seen in Fig. 3 (D and E), where columns capture the heterogeneity among target protein activity across single cells within and between a cell population, as well as detection of enzyme activity heterogeneity across the Ag-6 panel within a single cell (across rows), which shows unique profiles. Principal components analysis (PCA) confirmed that scADPL profiles could be used to cluster cells according to their molecular phenotype, as in the case of aggressive (SKOV3) and nonaggressive (OVCAR3) ovarian cancer cell lines (Fig. 3F). Together, these data capture the enzyme heterogeneity that exists both across single cells for an

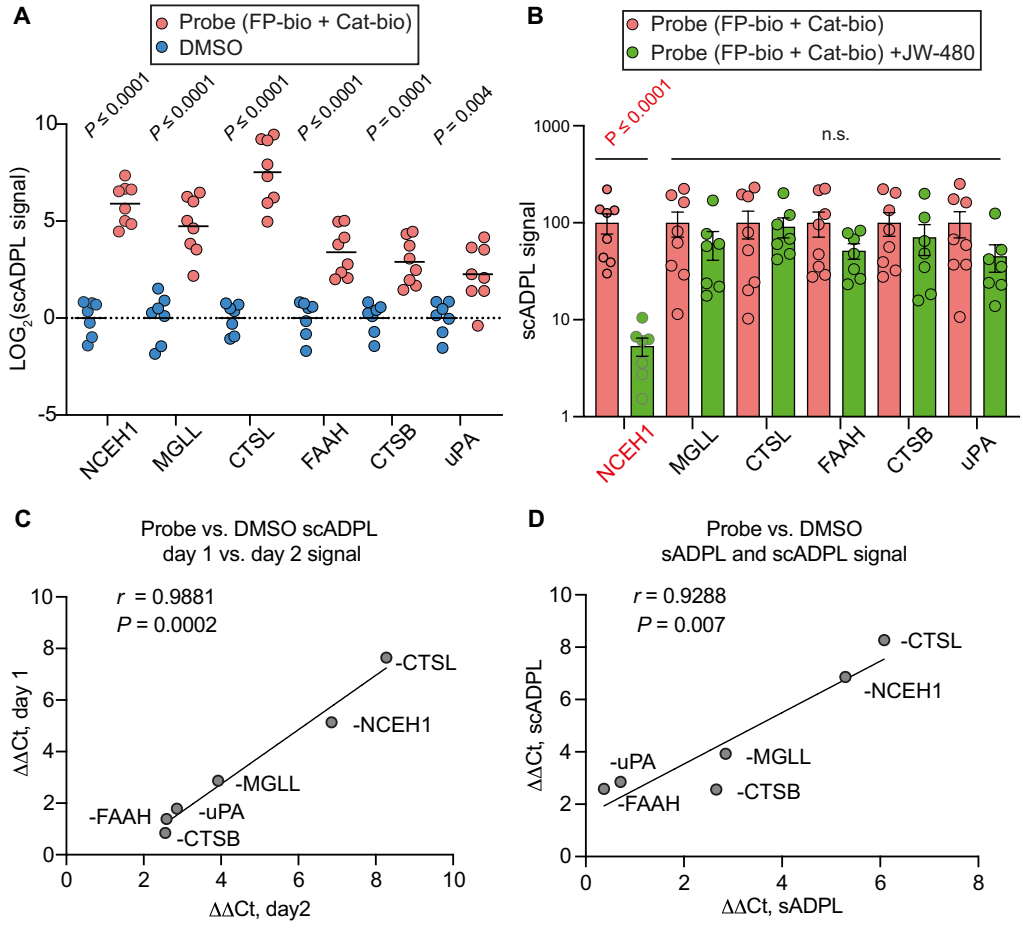

Fig. 2. Multiplexed scADPL quantification of activity signatures in isolated, single cells. (**A**) Simultaneous quantification of six enzyme targets from two families in dual-probe–treated (e.g., "Probe," 5 μM Cat-bio and 2 μM FP-bio) versus vehicle-treated SKOV3 cells. Each point represents a single qPCR scADPL measurement for that target in an isolated cell (all measurements shown are in the same $n = 8$ single cells). Mean relative scADPL signal shown as horizontal line. (**B**) scADPL quantification of six enzyme targets as shown in (A) with or without pretreatment with a selective inhibitor of one target, NCEH1, highlighted in red. Individual data points represent single scADPL target measurements from isolated single cells; all measurements are in the same $n = 7$ and $n = 8$, 2 μM JW480-treated and untreated cells, respectively. Bar graphs represent the mean relative ADPL signal normalized to 100 for dual-probe–treated samples without pretreatment of JW480. (**C**) Correlation plots of relative multiplexed scADPL activity measurements on dual-probe–treated SKOV3 cells on two separate days. Spearman's $r = 0.9881$. (**D**) Correlation plots of relative multiplexed activity measurements determined for each target in SKOV3 cells using scADPL or bulk sADPL measurement from many cells. Plots depict the average $\Delta\Delta C_T$ value for each target comparing dual-probe–treated cells and vehicle-treated cells measured on different days (C) or comparing scADPL and bulk sADPL workflows (D). sADPL and scADPL data points in (D) represent the mean from $n = 2$ and $n = 1$ technical replicate measures, respectively, each from a representative biological experiment repeated three times. Data in (A) and (B) compared with Student's two-way *t* test; n.s., not significant.

enzyme target and within an isolated single cell for the Ag6 panel, which can be used to differentiate cell type, tumor of origin, and tumor aggressiveness.

Single-cell profiling of samples from patients with BC identifies an activity signature correlated with metastatic phenotype

We next applied scADPL to measure activity signatures in complex, sample-limited tumor biopsies and isolated tumor cells from patients. We first chose to profile the activity of our six-enzyme aggressiveness panel (Ag-6) in live patient-derived organoids (PDOs) from primary and metastatic tumors obtained from either (i) six patients with triple-negative breast cancer (TNBC), enabling "between-patient" comparisons; or (ii) multiple tumors from one hormone refractory, estrogen receptor–positive (ER+) BC patient with metastatic BC, enabling "within-patient" comparison (Fig. 4A). We chose to use PDOs as a model to compare single-cell and bulk ADPL measurements with the same samples as a proof of concept.

We first profiled the Ag-6 panel in four distinct cell lines (MCF10A and TNBC cell lines HCC70, MDA-MB-231, and BM1), each representing a different stage in the continuum from noncancerous breast epithelium to metastatic lesion [MCF10A as noncancerous breast epithelium, HCC70 as normal BC, MDA-MB-231 as aggressive tumor cells having undergone epithelial-to-mesenchymal transition (EMT), and BM1 as a formed metastatic lesion] (*45*–*47*). We observed relatively low levels of Ag-6 enzyme activity in MCF10A and HCC70 cells, with a significant spike in activity in the MDA-MB-231 cell population (Fig. 4B). Activity levels of NCEH1 and

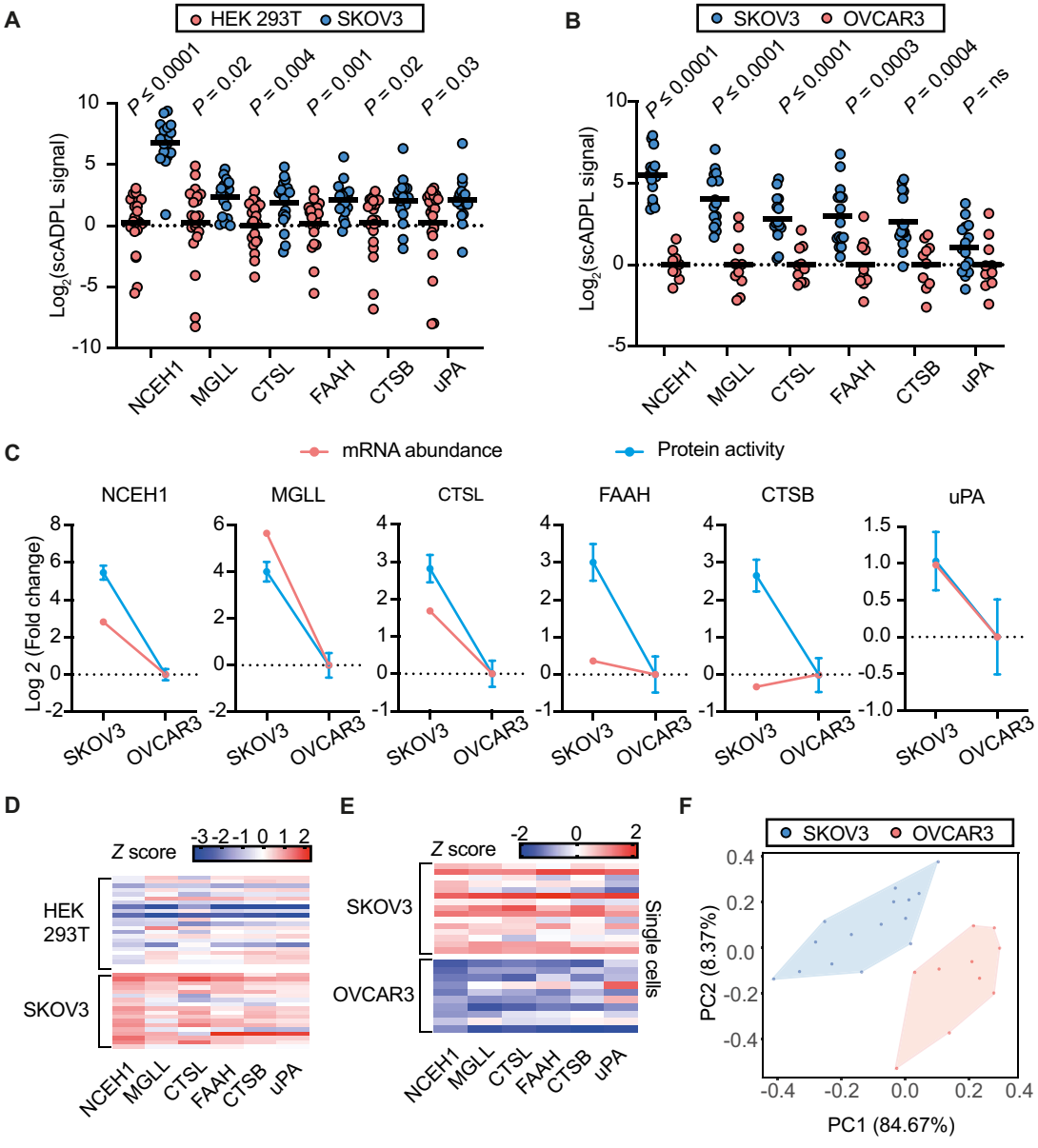

Fig. 3. scADPL quantifies multi-protein activity signatures and heterogeneity in single cells. (**A** and **B**) Multiplexed scADPL measurements in cell lines from different tissues of origin [i.e., HEK293T versus SKOV3 (A)] or the same tissue of origin [i.e., SKOV3 versus OVCAR3 (B)]. Each point represents a single qPCR scADPL measurement for that target in an isolated cell (all measurements shown are in the same dual-probe–treated single cells). Mean relative scADPL signal shown as horizontal line normalized to activity level in HEK293T (A) and OVCAR3 (B). Measurements are normalized to RPE internal control for each cell. Individual data points represent individual cells and the horizontal line represents activity mean. Each graph is representative of two independent biological replicates, with each target consisting of $n > 10$ isolated single cells. (**C**) Plots of relative mRNA abundance and active protein levels of the Ag-6 panel between the cell lines SKOV3 and OVCAR3 (B). mRNA measurements were obtained from the online repository, The Human Protein Atlas (https://proteinatlas.org) (*51*) and protein activity (in blue) of each Ag-6 panel member measured using scADPL. (**D** and **E**) Heatmaps of scADPL activity measurement *Z* scores within single cells. Each row within the heatmap represents activity measurements in the same cell; columns show activity across cells for a single target protein of interest. (**F**) PCA dimensional reduction performed using scADPL activity profiles in SKOV3 and OVCAR3 cells from (B). Clusters are highlighted in blue and red, with each data point representing a single cell. Data in (A) and (B) compared with Student's two-way *t* test; n.s., not significant.

uPA remained high while the activity of the other four members was reduced in the already-metastasized BM1 cells relative to their parent MDA-MB-231 cells. We also compared the activity level profiles to mRNA abundance reported in The Human Protein Atlas for these cell lines. Similar to the previous cell line case above, we observed that mRNA and active protein levels were generally correlated for some targets, while others showed starkly different profiles (fig. S4).

Having established a baseline in TNBC cell lines, we next profiled Ag-6 activity in organoids derived from primary and metastatic tumor resections from patients with TNBC (table S1). We observed higher Ag-6 activity in all metastatic cells relative to primary tumor cells, with the highest activity observed in two liver metastases (Fig. 4C and fig. S5). Next, we profiled organoids derived from two pleural effusions (i.e., disseminated cancer cells) and one established

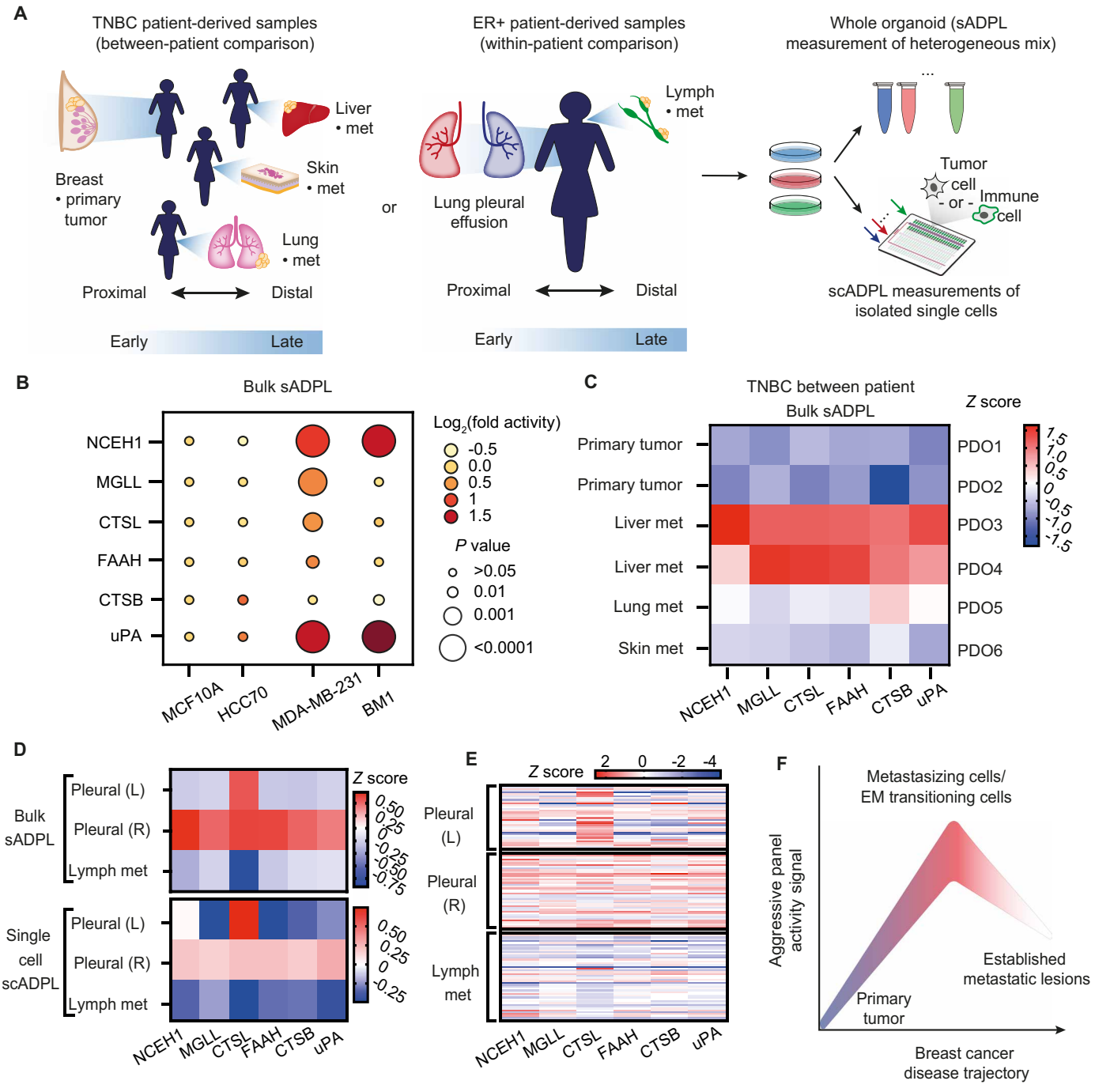

Fig. 4. scADPL detects enzyme activity signatures in tumor organoids derived from patients with BC. (**A**) Primary or metastatic tumor biopsies from several patients with TNBC (left) or a single ER+ patient (right) were used to generate heterogeneous organoids before bulk sADPL on organoid mixtures (top) or scADPL profiling of dissociated single cells (bottom). (**B**) Multiplexed sADPL quantification of the Ag-6 panel activity in four TNBC cell lines. Normalized activity is plotted for each target relative to activity measured in MCF10A cells from $n = 3$ biological replicates. (**C**) Multiplexed sADPL quantification of Ag-6 panel target activities in six different fresh PDOs derived from patient primary and metastatic tumor sites, as listed. Heatmap depicts relative activity Z scores obtained from $n = 4$ independent replicates. (**D**) Heatmap depiction of Ag-6 target activity levels (Z scores, representative of $n = 2$ biological replicates) measured by multiplexed sADPL and scADPL profiling of intact organoids and isolated single cells, respectively. Pleural effusion and lymph node metastasis samples were collected from the same ER+ patient. Individual target quantifications in each sADPL reaction or single-cell measurements were normalized to spike-in control R-phycoerythrin (RPE); relative activity Z scores in (C) and (D) were calculated by normalizing within each target to Primary—PDO1 and Lymph met samples, respectively. (**E**) Heatmaps of scADPL activity measurement Z scores in the left and right pleural effusion and the lymph metastasis. Each row within the heatmap represents a single cell, with columns plotting the activity of the indicated target within that cell. (**F**) General schematic depiction of Ag-6 activity signature changes in BC cell progression supported by data in this study. Ag-6 activity signature increases in cells that have undergone EMT or that have increased metastatic potential, and either remain elevated or slightly decrease in established metastatic BC lesions.

lymph node metastatic lesion taken from the same patient with ER+ BC. We performed multiplexed Ag-6 profiling with bulk sADPL, but to confirm measurement in tumor cells only, we also analyzed samples by scADPL. A key benefit of the scADPL platform is the on-chip staining and real-time visualization of cell morphology and/or other molecular markers. Here, we detected CD45+ cells as a filter to prevent inadvertent activity signature contamination from isolated immune cells. This is only possible with microfluidics-aided scADPL and could be expanded out to other cellular markers to identify a variety of cell types within biological samples (fig. S6). We observed the highest Ag-6 activity profile again in organoid cells established from pleural effusion relative to the organoid cells established from lymph node metastatic lesion. This generally agrees with the cell line studies showing the highest activity in disseminating MDA-MB-231 cells that were derived from a patient pleural effusion (Fig. 4, D and E, and fig. S7) (*48*), and this general trend was observed in both the single-cell and bulk ADPL measurements. The left pleural effusion was obtained before the right pleural effusion and the lymph node biopsy, likely during the early stages of metastasis detection, and this sample exhibits greater intertarget heterogeneity among the three PDO samples and a significant increase in CTSL activity. A general increase in Ag-6 activity and a decrease in variability between targets is observed in right pleural effusion sample, which was collected at a later stage in disease progression. A similar reduction in variability is also observed in lymph node metastases. In addition, mirroring our findings from cell culture analysis, the lymph metastasis also demonstrated a general decrease in Ag-6 activity, although the true tumor progression timeline within this patient is unknown (Fig. 4E and fig. S7). Together, these data confirm that scADPL and bulk ADPL profiling can be applied directly to low-abundance patient samples and isolated single cells for high-resolution molecular phenotyping. Moreover, we have identified an Ag-6 enzyme panel that correlates with metastatic and/or EMT in both BC cell lines and primary patient tissues (Fig. 4F).

DISCUSSION

Here, we present an automated chemoproteomic method, scADPL, which uses activity-based probes to detect and quantify endogenous protein activity state in single cells. To our knowledge, these are the first multiplexed measurements of this type. The scADPL platform is inherently modular, such that activity probes (and therefore target protein families), specific proteins of interest, cell types, multiplexing schemes, and microfluidic platforms could be interchanged for specific applications. Here, we focused on a multiplexed panel of previously interrogated cancer-associated enzymes (the Ag-6 panel) in the serine hydrolase and cathepsin protease families. We demonstrated quantitative precision and accuracy by comparing scADPL measurements between known cell types, inhibitor treatments, and across detection schemes. The microfluidic device used in this work enables in-line, automated processing of the scADPL workflow from cell capture to oligonucleotide barcode elution (Fig. 1). In principle, scADPL should be readily adapted to other microfluidic or robotic devices and formats, which could further reduce sample processing time and increase parallel sample processing. Moreover, while we demonstrate the potential to robustly detect target enzyme activity using qPCR, future work to increase multiplexed barcode deconvolution in the same sample reactions should be explored to increase multiplexing capacity (which was not a goal in this study) and increase throughput.

There are several limitations to our study. First, the qPCR readout currently requires splitting of single-cell contents for parallel amplicon detection and quantification. This could provide an upper limit on the number of targets that can be accurately profiled in single cells. Other quantification methods could likely improve or obviate this limitation. Second, as with other proximity ligation approaches, we rely on high-quality barcoded antibodies, which can be a limitation due to availability and performance of antibodies. However, because the chemical probe(s) used in scADPL already serve to anchor one-half of the barcoding scheme, we believe that the success rate of finding a suitable target-specific antibody is higher than finding two distinct antibodies, as is necessary in proximity ligation approaches that only measure bulk protein abundance. In all cases, reagent availability and quality control are important. Last, we demonstrated the proof-of-concept application of scADPL to two protein classes for which previous probe designs could be adapted for live-cell treatments and downstream integration into ADPL. Expansion to other protein families with existing and new probes is supported by the modularity of the ADPL platform and could extend the range of targets and biology that can be studied using this method.

Last, we demonstrated the direct molecular phenotyping capabilities of the scADPL platform to identify metastasis-associated activity profiles in BC cell lines and PDOs. Using cell lines, we identified the consistent increase in Ag-6 panel activity in BC cells that have undergone or are undergoing EMT and/or metastasis (Fig. 4, C to E). This general profile was also observed in metastatic tumor-derived cells from the same patient and between a group of tissues collected from multiple patients. The patient samples used here were not powered or controlled to confirm the specificity or predictive nature of this profile but were focused on testing whether scADPL profiling could accurately and precisely measure activity profiles correlated with disease state. Future studies to expand this testing cohort in BC and other cancers are warranted to determine the robust and potential diagnostic utility of the Ag-6 panel in understanding cancer progression and treatment. Beyond the specific targets studied here, a general limitation with averaged protein abundance or activity signatures obtained via traditional (e.g., gel or mass spectrometry based) or other bulk methods like sADPL is the large cell input requirement (e.g., thousands to millions of cells) upstream of time-intensive and low-throughput activity-based processing and analysis workflows. This fundamentally limits the ability to profile many sample types, such as small patient sample biopsies or circulating cells. The aggregate analysis of heterogeneous cell mixtures also prevents bona fide detection of activity profiles from specific cell types, such as the patient-derived BC cells measured here. The scADPL approach described here provides a specific solution to many of these issues, as well as a general framework for expansion to interrogate other additional protein targets, families, and activity signatures more broadly in basic and translational settings.

MATERIALS AND METHODS

Reagents and general equipment

All the chemicals were purchased from Sigma-Aldrich, unless otherwise mentioned and were used as received. NCEH1 polyclonal antibody was previously reported (*33*, *36*). Other commercial antibodies were purchased from Abcam (no. ab58802, anti-cathepsin B; no. ab54615, anti-FAAH1; no. 24701, anti-MGLL; no. 24121, anti-urokinase; no. 34721, anti-RPE) and from R&D Systems (no. AF952-SP, anti-cathepsin L).

Streptavidin was purchased from Leinco Technologies (no. S203) and R-phycoerythrin was purchased from Thermo Fisher Scientific (no. P801). SYBR gold nucleic acid stain and NuPAGE Novex 4% to 12% bis-tris protein gels were purchased from Thermo Fisher Scientific (no. S11494 and no. NP0322BOX, respectively). Oligonucleotides and Taq-Man probe for qPCR were purchased from Integrated DNA Technologies. DSS linker and polyadenylic acid were purchased from Sigma-Aldrich (no. S11494 and no. P9403, respectively). Bicinchoninic acid (BCA) and micro-BCA assays were purchased from Thermo Fisher Scientific (no. 23225 and no. 23235, respectively). Immunoglobulin G (IgG) was purchased from Thermo Fisher Scientific (no. 02-6202). Thermo Fisher Scientific NanoDrop One^C was used for performing absorption measurements. Luna universal probe qPCR master mix (no. M3004E) and Phusion high-fidelity DNA polymerase (no. M0503L) were purchased from New England Biolabs. Ampligase was purchased from Lucigen (no. E0001-5D3).

Cell lines

HeK293T, HCC70, BM1, and MDA-MB-231 cells were grown in RPMI 1640, SKOV3, OVCAR3, and MCF 10A cell lines grown in Dulbecco's modified Eagle's medium (DMEM)–F12 supplemented with 10% fetal bovine serum (FBS; Thermo Fisher Scientific) and 1% penicillin/streptomycin (Hyclone). All cells except BM1 cells were procured from the American Type Culture Collection and were not short tandem repeat (STR) profiled. BM1 cells were kindly provided by Dr. Marsha Rosner from the University of Chicago. Cells were grown in a water-jacketed humidified incubator at 37°C with 5% CO_2. All cells tested negative for mycoplasma contamination.

PDO development and preparation

The procurement of biospecimens for the generation of breast cancer (BC) patient-derived organoids (PDOs) has been performed according to the approved institution review board protocol (16352A) with a signed patient consent. All patient samples and clinical information related to the samples have been deidentified. Fresh core needle biopsy samples or cells from pleural effusions were remnant specimens collected without compromising required diagnostic procedures. PDOs were established as previously described (*49*). Briefly, tissue obtained from a core biopsy was enzymatically digested for 1 hour to generate cell suspension. Cells from pleural effusions were collected by centrifugation at 450*g* for 10 min and washed in Advanced DMEM-F12 containing 10 mM Hepes, 1× Glutamax, and penicillin/streptomycin (AdvM+). Pelleted cells were mixed with Matrigel (MG), plated into prewarmed 24-well plates to allow MG to solidify at 37°C and supplemented with BC PDO media to grow organoids (*49*). To prevent misidentification and cross-contamination, each PDO sample was cultured in a separate, appropriately labeled dish, and the identity of PDOs was confirmed by fingerprinting using the AmpFLSTR Identifier PCR Amplification Kit. All PDOs were tested for mycoplasma contamination. Once PDOs reached 50 to 100 mm size, they were collected for subsequent experimental procedures. To dissociate from MG, PDOs were incubated with Dispase at 37°C for 20 min, washed twice with AdvM+, and centrifuged at 450*g* for 5 min. To obtain a single-cell suspension, the PDO pellet was incubated with TrypLE at 37°C for 5 to 10 min. Trypsinization was stopped with 2% FBS, and cells were washed twice with AdvM+, passed through a 40-mm cell strainer, and centrifuged at 450*g* for 5 min. Cells were resuspended in 500 μl of BC PDO media and kept on ice before activity profiling on the chip.

Preparation of cell lines and PDO lysates for soluble ADPL measurements as well as standardization measurements on microfluidic device

Cells were treated with a 5 μM cathepsin family-wide probe for 2 hours and 2 μM family-wide serine hydrolase probe FP-Biotin for 30 min at 37°C in RPMI or DMEM supplemented with 10% FBS. Single-cell PDO suspension in BC PDO media was treated with a 5 μM cathepsin family-wide probe for 2 hours and 2 μM family-wide serine hydrolase probe FP-Biotin for 30 min at 37°C. Cells were washed with phosphate-buffered saline (PBS) and then lysed in MCP buffer, and the protein concentration was determined by a BCA assay.

Preparation of cell lines and PDO for single-cell microfluidic experiment

(i) Cells and (ii) single-cell PDO suspension were treated as mentioned above. Cells and PDOs were washed with PBS. To obtain single-cell suspension, (i) the cells were then incubated with Trypsin for 2 min. The digestion was then quenched by adding fresh RPMI or DMEM supplemented with FBS. The cells were resuspended in PBS and diluted such that there are around 50,000 to 100,000 cells in 1 ml and they are loaded on the microfluidic device. (ii) The PDOs were resuspended in PBS supplemented with 2% FBS. The cells were then incubated with anti-CD45 antibody conjugated to fluorescein isothiocyanate (FITC) for 30 min on ice, washed twice, and loaded onto the microfluidic device.

Lysis buffer optimization

For optimization of lysis condition, the cells were lysed in Pierce, CST, TM, and MCP buffers. MCP lysis buffer was prepared with 25 mM tris (pH 7.5), 150 mM NaCl, 1 mM EDTA, 1 mM EGTA, 0.5% Triton X-100, and 0.5% sodium deoxycholic. CST lysis buffer was prepared with 25 mM tris (pH 7.5), 150 mM NaCl, 1 mM EDTA, 1 mM EGTA, and 1% Triton X-100. Pierce lysis buffer was prepared with 25 mM tris (pH 7.5), 150 mM NaCl, 1 mM EDTA, 1 mM EGTA, 1% NP-40, and 5% glycerol. TM buffer was prepared with 10 mM $MgSO_4$, 10 mM tris (pH 7.5), and 5 μM $CaCl_2$.

Single-cell enzyme and bulk activity profiling on chip

Single cells were lysed in MCP lysis buffer with the addition of the spike in control R-phycoerythrin on the chip. For the bulk experiments on the chip, the cells were lysed in MCP buffer by sonication, following which the protein concentration was measured by BCA assay. The lysates were diluted to the same concentration and then directly loaded into the chip. For on-chip analysis, this is followed by on-chip conjugate incubation for 2 hours and ligation for 45 min to give the desired ligation product. In this manner, the no-probe control sample and probe-treated samples both receive the ligation oligonucleotide and the probe recognition reagents (ab-conjugates and SA-conjugates). The ligated product is flushed out using 9 μl of water and then preamplified using 11 μl of the preamplification mixture (2.5× buffer, 100 nM primers, 200 μM dNTPs, and 9 U Phusion high fidelity DNA polymerase). The preamplified product is then subjected to qPCR analysis as mentioned in the multiplexed sADPL protocol.

Multiplexed soluble activity profiling with sADPL

A threefold dilution series of the lysates were used for the optimization experiments, and for the experiments with organoids, a final concentration of 0.1 mg/ml was used. The probes were first treated with

PEG-8000 (polyethylene glycol, molecular weight 8000) to a final concentration of 5% and then spun down at 4000 rpm for 30 min to remove any potential assay interference. Lysate (2 μl) was mixed with 2 μl of the ADPL probe mixture such that we ended up with a final concentration of 200 pM of the enzyme-specific antibody oligo conjugate (both for ADPL and PLA) and 4000 pM of the streptavidin oligo conjugate in PBS containing poly-A (20 μg/ml), 2 mM EDTA, 1% BSA, and 0.05% goat IgG. This mixture was then incubated at 37°C for 1 hour, followed by the addition of 116 μl of the ligation mixture composed of 100 nM splint oligonucleotide, 0.05 U of ampligase, 0.3 mM NAD^+, 10 mM DTT, 20 mM tris-HCl (pH 8.3), 50 mM KCl, and 1.5 mM $MgCl_2$. Ligation incubation occurred at 40°C for 30 min. The ligated products were then subjected to preamplification PCR by mixing 5 μl of the ligated mixture to 20 μl of the preamplification mixture (2.5× buffer, 100 nM primers, 200 μM dNTPs, and 9 U Phusion high fidelity DNA polymerase) and amplified for 18 cycles. The preamplified products were extracted using 75 μl of TE buffer and subjected to qPCR. The extracted preamplification mixture (4.5 μl) was added to 5.5 μl of qPCR mixture (0.9 μM primers and 0.45 μM Taqman probe in Luna Universal Probe qPCR Master Mix). Samples were run on a CFX384 Real-Time System (384-well plates). After the PCR, the values were either normalized to PBS (for simpler optimization experiments) or normalized to RPE (for more complex experiments) (*50*). Individual cells for scADPL measurements and replicates for sADPL measurements with internal control RPE values that were 2 SDs away from the mean were considered spurious outliers introduced due to technical errors and were omitted from further analysis.

Microfluidic chip fabrication

The microfluidic chip molds were designed with AutoCAD (Autodesk, USA) and were used as blueprints with Heidelberg MLA 150 Direct Write Lithographer (Heidelberg Instruments Mikrotechnik GmbH, Germany) to expose UV light on 4-inch photoresist-coated silicon wafers to define chip features. The microfluidic chip consists of features of different photoresist heights: 18-mm AZ40XT (MicroChem, USA) spun at 1976*g*, 22-mm SU-8-3025 spun at 1372*g*, and 70 mm coated with two layers of SU-8-3025—the first layer spun at 1372*g* and the second layer spun at 448*g*. The AZ layer forms a rounded dome-like shape after overnight reflow. The valve-based microfluidic chip consists of three layers: fluidic layer, control layer, and glass slide at the bottom. Here, we used a "push-up" chip configuration, in which a fluidic layer is thick and bonded on top of a thin control layer that is bonded to a glass slide. The microfluidic chip is made of a polymer material called polydimethylsiloxane (PDMS). Before casting a PDMS device out of the molds, the molds were first treated with chlorotrimethylsilane (cat. no. 92360, Sigma-Aldrich, USA) for 15 min in a fume hood, which ensured the molds were nonsticky to PDMS, and thus preserve the features on molds for long-term usage. To cast the thick layer, ~72 g of PDMS was prepared by mixing the base and the curing agent at 10:1 ratio (66 g of base and 6.6 g of curing agent). The mixture was then thoroughly mixed and degassed automatically (RTV-615, Momentive Specialty Chemicals, USA). The prepared PDMS was then poured over the coated mold and degassed again. To cast the thin layer, 11 g of PDMS was prepared following the same ratio mentioned before. Then, the PDMS was poured onto coated mold and spun at 448*g* for 1 min. The PDMS-coated thin layer was placed on a level surface for about 15 min to let the PDMS reflow and form an even surface. The thin layers were incubated at 80°C for at least 45 min, while the thick layers were incubated overnight at the same temperature. The thick layer was then peeled off the fluidic layer mold, punched at the fluidic inlets/outlets, and aligned and bonded onto the thin layer with both bonding surfaces treated with oxygen plasma for 18 s (oxygen input pressure 860 mtorr, Harrick Plasma, USA). The aligned assemble was incubated at 80°C overnight, then it was peeled off the control layer mold, and was punched again at the control inlets. The retrieval outlets were punched with a 1930-μm–inner diameter biopsy punch (CR0950765N13R4, Syneoco, USA), and the rest of the inlets/outlets were punched with a 710-mm–inner diameter biopsy punch (CR0350255N20R4, Syneoco, USA). Last, the assemble was bonded to a clean and dry glass slide (127.76 mm × 85.48 mm × 1 mm) with air plasma for 45 s (turn on the air plasma at a pressure of 800 mtorr, then briefly refill the chamber with air every 10 s). The final bonded device was then incubated at 80°C for at least overnight to ensure tight bonding.

Supplementary Materials

The PDF file includes:

Figs. S1 to S7
Table S1
Legend for data s1

Other Supplementary Material for this manuscript includes the following:

Data S1

REFERENCES AND NOTES

1. R. Stark, M. Grzelak, J. Hadfield, RNA sequencing: The teenage years. *Nat. Rev. Genet.* **20**, 631–656 (2019).
2. W. Chung, H. H. Eum, H. O. Lee, K. M. Lee, H. B. Lee, K. T. Kim, H. S. Ryu, S. Kim, J. E. Lee, Y. H. Park, Z. Kan, W. Han, W. Y. Park, Single-cell RNA-seq enables comprehensive tumour and immune cell profiling in primary breast cancer. *Nat. Commun.* **8**, 15081 (2017).
3. A. Mortazavi, B. A. Williams, K. McCue, L. Schaeffer, B. Wold, Mapping and quantifying mammalian transcriptomes by RNA-Seq. *Nat. Methods* **5**, 621–628 (2008).
4. L. Vistain, H. van Phan, B. Keisham, C. Jordi, M. Chen, S. T. Reddy, S. Tay, Quantification of extracellular proteins, protein complexes and mRNAs in single cells by proximity sequencing. *Nat. Methods* **19**, 1578–1589 (2022).
5. L. Keller, K. Pantel, Unravelling tumour heterogeneity by single-cell profiling of circulating tumour cells. *Nat. Rev. Cancer* **19**, 553–567 (2019).
6. S. P. Gygi, Y. Rochon, B. R. Franza, R. Aebersold, Correlation between protein and mRNA abundance in yeast. *Mol. Cell. Biol.* **19**, 1720–1730 (1999).
7. E. J. Foss, D. Radulovic, S. A. Shaffer, D. M. Ruderfer, A. Bedalov, D. R. Goodlett, L. Kruglyak, Genetic basis of proteome variation in yeast. *Nat. Genet.* **39**, 1369–1375 (2007).
8. M. Gry, R. Rimini, S. Strömberg, A. Asplund, F. Pontén, M. Uhlén, P. Nilsson, Correlations between RNA and protein expression profiles in 23 human cell lines. *BMC Genomics* **10**, 365 (2009).
9. A. Ghazalpour, B. Bennett, V. A. Petyuk, L. Orozco, R. Hagopian, I. N. Mungrue, C. R. Farber, J. Sinsheimer, H. M. Kang, N. Furlotte, C. C. Park, P. Z. Wen, H. Brewer, K. Weitz, D. G. Camp, C. Pan, R. Yordanova, I. Neuhaus, C. Tilford, N. Siemers, P. Gargalovic, E. Eskin, T. Kirchgessner, D. J. Smith, R. D. Smith, A. J. Lusis, Comparative analysis of proteome and transcriptome variation in mouse. *PLOS Genet.* **7**, e1001393 (2011).
10. B. Zhang, J. Wang, X. Wang, J. Zhu, Q. Liu, Z. Shi, M. C. Chambers, L. J. Zimmerman, K. F. Shaddox, S. Kim, S. R. Davies, S. Wang, P. Wang, C. R. Kinsinger, R. C. Rivers, H. Rodriguez, R. R. Townsend, M. J. C. Ellis, S. A. Carr, D. L. Tabb, R. J. Coffey, R. J. C. Slebos, D. C. Liebler; the NCI CPTAC, Proteogenomic characterization of human colon and rectal cancer. *Nature* **513**, 382–387 (2014).
11. C. Walsh, *Posttranslational Modification of Proteins: Expanding Nature's Inventory* (Roberts and Co. Publishers, 2006), pp. xxi, 490 p.
12. S. Ramazi, J. Zahiri, Posttranslational modifications in proteins: Resources, tools and prediction methods. *Database* **2021**, baab012 (2021).
13. T. Pawson, P. Nash, Protein-protein interactions define specificity in signal transduction. *Genes Dev.* **14**, 1027–1047 (2000).
14. J. Westermarck, J. Ivaska, G. L. Corthals, Identification of protein interactions involved in cellular signaling. *Mol. Cell. Proteomics* **12**, 1752–1763 (2013).
15. R. E. Moellering, B. F. Cravatt, Functional lysine modification by an intrinsically reactive primary glycolytic metabolite. *Science* **341**, 549–553 (2013).
16. I. Piazza, K. Kochanowski, V. Cappelletti, T. Fuhrer, E. Noor, U. Sauer, P. Picotti, A map of protein-metabolite interactions reveals principles of chemical communication. *Cell* **172**, 358–372.e23 (2018).

17. H. J. Forman, F. Ursini, M. Maiorino, An overview of mechanisms of redox signaling. *J. Mol. Cell. Cardiol.* **73**, 2–9 (2014).
18. Y. M. W. Janssen-Heininger, B. T. Mossman, N. H. Heintz, H. J. Forman, B. Kalyanaraman, T. Finkel, J. S. Stamler, S. G. Rhee, A. van der Vliet, Redox-based regulation of signal transduction: Principles, pitfalls, and promises. *Free Radic. Biol. Med.* **45**, 1–17 (2008).
19. C. M. Agapakis, P. M. Boyle, P. A. Silver, Natural strategies for the spatial optimization of metabolism in synthetic biology. *Nat. Chem. Biol.* **8**, 527–535 (2012).
20. D. A. Fletcher, R. D. Mullins, Cell mechanics and the cytoskeleton. *Nature* **463**, 485–492 (2010).
21. A. M. Sadaghiani, S. H. Verhelst, M. Bogyo, Tagging and detection strategies for activity-based proteomics. *Curr. Opin. Chem. Biol.* **11**, 20–28 (2007).
22. B. F. Cravatt, A. T. Wright, J. W. Kozarich, Activity-based protein profiling: From enzyme chemistry to proteomic chemistry. *Annu. Rev. Biochem.* **77**, 383–414 (2008).
23. R. E. Moellering, B. F. Cravatt, How chemoproteomics can enable drug discovery and development. *Chem. Biol.* **19**, 11–22 (2012).
24. Y. Liu, M. P. Patricelli, B. F. Cravatt, Activity-based protein profiling: The serine hydrolases. *Proc. Natl. Acad. Sci. U.S.A.* **96**, 14694–14699 (1999).
25. G. M. Simon, B. F. Cravatt, Activity-based proteomics of enzyme superfamilies: Serine hydrolases as a case study. *J. Biol. Chem.* **285**, 11051–11055 (2010).
26. M. P. Patricelli, A. K. Szardenings, M. Liyanage, T. K. Nomanbhoy, M. Wu, H. Weissig, A. Aban, D. Chun, S. Tanner, J. W. Kozarich, Functional interrogation of the kinome using nucleotide acyl phosphates. *Biochemistry* **46**, 350–358 (2007).
27. Q. Zhao, X. Ouyang, X. Wan, K. S. Gajiwala, J. C. Kath, L. H. Jones, A. L. Burlingame, J. Taunton, Broad-spectrum kinase profiling in live cells with lysine-targeted sulfonyl fluoride probes. *J. Am. Chem. Soc.* **139**, 680–685 (2017).
28. A. Saghatelian, N. Jessani, A. Joseph, M. Humphrey, B. F. Cravatt, Activity-based probes for the proteomic profiling of metalloproteases. *Proc. Natl. Acad. Sci. U.S.A.* **101**, 10000–10005 (2004).
29. D. Kato, K. M. Boatright, A. B. Berger, T. Nazif, G. Blum, C. Ryan, K. A. H. Chehade, G. S. Salvesen, M. Bogyo, Activity-based probes that target diverse cysteine protease families. *Nat. Chem. Biol.* **1**, 33–38 (2005).
30. E. Weerapana, C. Wang, G. M. Simon, F. Richter, S. Khare, M. B. D. Dillon, D. A. Bachovchin, K. Mowen, D. Baker, B. F. Cravatt, Quantitative reactivity profiling predicts functional cysteines in proteomes. *Nature* **468**, 790–795 (2010).
31. M. L. Matthews, L. He, B. D. Horning, E. J. Olson, B. E. Correia, J. R. Yates III, P. E. Dawson, B. F. Cravatt, Chemoproteomic profiling and discovery of protein electrophiles in human cells. *Nat. Chem.* **9**, 234–243 (2017).
32. J. W. Chang, J. E. Montgomery, G. Lee, R. E. Moellering, Chemoproteomic profiling of phosphoaspartate modifications in prokaryotes. *Angew. Chem. Int. Ed. Engl.* **57**, 15712–15716 (2018).
33. G. Li, J. E. Montgomery, M. A. Eckert, J. W. Chang, S. M. Tienda, E. Lengyel, R. E. Moellering, An activity-dependent proximity ligation platform for spatially resolved quantification of active enzymes in single cells. *Nat. Commun.* **8**, 1775 (2017).
34. G. Li, R. E. Moellering, A concise, modular antibody-oligonucleotide conjugation strategy based on disuccinimidyl ester activation chemistry. *Chembiochem* **20**, 1599–1605 (2019).
35. G. Li, R. E. Moellering, Chemical probes for spatially resolved measurement of active enzymes in single cells. *Methods Enzymol.* **628**, 243–262 (2019).
36. G. Li, M. A. Eckert, J. W. Chang, J. E. Montgomery, A. Chryplewicz, E. Lengyel, R. E. Moellering, Ultrasensitive, multiplexed chemoproteomic profiling with soluble activity-dependent proximity ligation. *Proc. Natl. Acad. Sci. U.S.A.* **116**, 21493–21500 (2019).
37. D. Martínez-Martín, G. Fläschner, B. Gaub, S. Martin, R. Newton, C. Beerli, J. Mercer, C. Gerber, D. J. Müller, Inertial picobalance reveals fast mass fluctuations in mammalian cells. *Nature* **550**, 500–505 (2017).
38. J. Lin, C. Jordi, M. Son, H. van Phan, N. Drayman, M. F. Abasiyanik, L. Vistain, H. L. Tu, S. Tay, Ultra-sensitive digital quantification of proteins and mRNA in single cells. *Nat. Commun.* **10**, 3544 (2019).
39. M. G. Paulick, M. Bogyo, Development of activity-based probes for cathepsin X. *ACS Chem. Biol.* **6**, 563–572 (2011).
40. K. P. Chiang, S. Niessen, A. Saghatelian, B. F. Cravatt, An enzyme that regulates ether lipid signaling pathways in cancer annotated by multidimensional profiling. *Chem. Biol.* **13**, 1041–1050 (2006).
41. D. K. Nomura, J. Z. Long, S. Niessen, H. S. Hoover, S. W. Ng, B. F. Cravatt, Monoacylglycerol lipase regulates a fatty acid network that promotes cancer pathogenesis. *Cell* **140**, 49–61 (2010).
42. M. A. Nouh, M. M. Mohamed, M. el-Shinawi, M. A. Shaalan, D. Cavallo-Medved, H. M. Khaled, B. F. Sloane, Cathepsin B: A potential prognostic marker for inflammatory breast cancer. *J. Transl. Med.* **9**, 1 (2011).
43. D. R. Sudhan, D. W. Siemann, Cathepsin L targeting in cancer treatment. *Pharmacol. Ther.* **155**, 105–116 (2015).
44. J. E. Testa, J. P. Quigley, The role of urokinase-type plasminogen activator in aggressive tumor cell behavior. *Cancer Metastasis Rev.* **9**, 353–367 (1990).
45. B. D. Lehmann, J. A. Bauer, X. Chen, M. E. Sanders, A. B. Chakravarthy, Y. Shyr, J. A. Pietenpol, Identification of human triple-negative breast cancer subtypes and preclinical models for selection of targeted therapies. *J. Clin. Invest.* **121**, 2750–2767 (2011).
46. X. Dai, H. Cheng, Z. Bai, J. Li, Breast cancer cell line classification and its relevance with breast tumor subtyping. *J. Cancer* **8**, 3131–3141 (2017).
47. J. Lee, A. E. Yesilkanal, J. P. Wynne, C. Frankenberger, J. Liu, J. Yan, M. Elbaz, D. C. Rabe, F. D. Rustandy, P. Tiwari, E. A. Grossman, P. C. Hart, C. Kang, S. M. Sanderson, J. Andrade, D. K. Nomura, M. G. Bonini, J. W. Locasale, M. R. Rosner, Effective breast cancer combination therapy targeting BACH1 and mitochondrial metabolism. *Nature* **568**, 254–258 (2019).
48. R. Cailleau, R. Young, M. Olivé, W. J. Reeves Jr., Breast tumor cell lines from pleural effusions. *J. Natl. Cancer Inst.* **53**, 661–674 (1974).
49. N. Sachs, J. de Ligt, O. Kopper, E. Gogola, G. Bounova, F. Weeber, A. V. Balgobind, K. Wind, A. Gracanin, H. Begthel, J. Korving, R. van Boxtel, A. A. Duarte, D. Lelieveld, A. van Hoeck, R. F. Ernst, F. Blokzijl, I. J. Nijman, M. Hoogstraat, M. van de Ven, D. A. Egan, V. Zinzalla, J. Moll, S. F. Boj, E. E. Voest, L. Wessels, P. J. van Diest, S. Rottenberg, R. G. J. Vries, E. Cuppen, H. Clevers, A living biobank of breast cancer organoids captures disease heterogeneity. *Cell* **172**, 373–386.e10 (2018).
50. M. Lundberg, S. B. Thorsen, E. Assarsson, A. Villablanca, B. Tran, N. Gee, M. Knowles, B. S. Nielsen, E. González Couto, R. Martin, O. Nilsson, C. Fermer, J. Schlingemann, I. J. Christensen, H. J. Nielsen, B. Ekström, C. Andersson, M. Gustafsson, N. Brunner, J. Stenvang, S. Fredriksson, Multiplexed homogeneous proximity ligation assays for high-throughput protein biomarker research in serological material. *Mol. Cell. Proteomics* **10**, M110.004978 (2011).
51. M. Uhlen, C. Zhang, S. Lee, E. Sjöstedt, L. Fagerberg, G. Bidkhori, R. Benfeitas, M. Arif, Z. Liu, F. Edfors, K. Sanli, K. von Feilitzen, P. Oksvold, E. Lundberg, S. Hober, P. Nilsson, J. Mattsson, J. M. Schwenk, H. Brunnström, B. Glimelius, T. Sjöblom, P. H. Edqvist, D. Djureinovic, P. Micke, C. Lindskog, A. Mardinoglu, F. Ponten, A pathology atlas of the human cancer transcriptome. *Science* **357**, eaan2507 (2017).

Acknowledgments: We thank all the patients who kindly donated samples. We thank S. Ahmadiantehrani for valuable suggestions during the writing process and proofreading assistance. We thank R. Romero for valuable suggestions with organoid handling. **Funding:** This work was supported by National Institutes of Health Chemical + Biology Training T32-GM144290 (to O.L.), National Cancer Institute P20CA233307 (to R.E.M. and O.I.O.), Alvin H. Baum Family Fund (to O.I.O.), Susan G. Komen Foundation Scholar Award (SAC210203) (to O.I.O.), Paul G. Allen Foundation Distinguished Investigator Award (to S.T.), National Institutes of Health grant GM127527 (to S.T.), National Institutes of Health grant DP2GM128199 (to R.E.M.), National Institutes of Health R01GM145852 (to R.E.M.), National Institutes of Health R33CA269094 (to R.E.M. and S.T.), Susan G. Komen Foundation Career Catalyst Research CCR 21663985 (to R.E.M.), and Alfred P. Sloan Foundation FG-2020-12839 (to R.E.M.). **Author contributions:** All authors reviewed the manuscript. Conceptualization: R.E.M. and S.T. Methodology: K.S.P., O.L., J.L., G.L., S.T., and R.E.M. Investigation: K.S.P., O.L., J.L., G.L., and O.K. Primary breast cancer tissue collection, organoid generation, and supervision: O.K., R.N., and O.I.O. Visualization: K.S.P., O.L., J.L., G.L., S.T., and R.E.M. Supervision: R.E.M. and S.T. Writing—original draft: K.S.P. and R.E.M. Writing—review and editing: K.S.P., O.L., S.T., and R.E.M. **Competing interests:** R.E.M. is a founder, consultant, and director of ReAx Biotechnologies Inc., which has licensed patents from the University of Chicago related to ADPL. All other authors declare that they have no competing interests. **Data and materials availability:** All data needed to evaluate the conclusions in the paper are present in the paper and/or the Supplementary Materials.

Submitted 7 April 2024
Accepted 18 September 2024
Published 23 October 2024
10.1126/sciadv.adp2622